

Research article

Comparative evaluation of drying methods for struvite produced from electrocoagulated source-separated urine: Implications for quality, energy and cost-effectiveness

Alisha Zaffar, Sivaraman Jayaraman, Parag Prakash Sutar, Paramasivan Balasubramanian *

Department of Biotechnology and Medical Engineering, National Institute of Technology Rourkela, Odisha, -769008, India

ARTICLE INFO

Handling editor: Jason Michael Evans

Keywords:

Struvite
Cost-effective
Energy
Drying kinetics
Electrocoagulation
Source-separated urine

ABSTRACT

Struvite precipitation from source-separated urine is crucial for waste utilization and sustainability. However, after precipitation, the high moisture content of struvite necessitates an additional drying process that can be costly and inefficient. In the present study, the performance of different drying methods—open sun drying, air drying, conventional drying (20–100 °C), and microwave drying (180–720 W) on the quality of struvite obtained from source-separated urine through electrocoagulation using Mg–Mg electrodes were evaluated. It was found that higher temperatures and power in the convective oven and microwave resulted in higher diffusivity (10^{-9} – $10^{-7} \text{ m}^2\text{s}^{-1}$), leading to reduced drying times. Different models were employed to comprehend the drying mechanism, and the one with the highest correlation coefficient ($R^2 = 0.99$) and the lowest statistical values was selected. The key findings indicated that higher power and temperature levels were more cost-effective. However, characterization of the dried struvite using X-ray diffraction and Fourier-transformed infrared spectroscopy, disintegration of struvite crystals at temperatures above 60 °C in the conventional oven and 180 W in the microwave oven was observed. Based on the results, we conclude that sun drying is a cost-effective and environmentally friendly alternative for drying struvite without compromising its quality.

1. Introduction

Struvite ($\text{MgNH}_4\text{PO}_4 \cdot 6\text{H}_2\text{O}$) is a market-attractive nutrient-rich product recovered from wastewater. It is sparingly soluble in water, makes it a potential slow fertilizer that can reduce the pressure on the depleting phosphorus reserves as well as tackle the problem of eutrophication and algal bloom (Rufí-Salís et al., 2020; Talboys et al., 2016). Human urine is a major contributor to phosphorus in wastewater, which, when recovered, can meet 10% of the world's total phosphorus demand (Mayer et al., 2016). The high phosphorus content in urine at alkaline pH can be converted to struvite by the addition of magnesium ions in the form of salts, anode, bittern, etc. (Bagastyo et al., 2022). Production of struvite from wastewater and its utilization in the agricultural field is a sustainable approach of resource recovery to attain circular economy (Preisner et al., 2022). However, struvite production is a multi-step process that involves synthesis, solid-liquid separation, and drying to form the solid, dense, and odorless residue, which can increase the cost of production (Zaffar et al., 2023). High capital during the installation and operational costs have limited the

implementation of struvite recovery plants. The operational cost includes the usage of different chemicals and the energy requirement for precipitation and downstream processing of struvite (Kim et al., 2021). The electrocoagulation technique reduces the chemical requirement, thus aiding in cost reduction during precipitation. The solid-liquid separation reduces the moisture content by a large amount; however, the precipitate contains sufficient water that cannot be directly used as fertilizer and requires an additional drying step. Hence, drying can affect the cost of downstream processing in large-scale production as well as the quality of struvite (Shaddel et al., 2019).

Drying of struvite is accompanied by various reactions, including the evaporation of water, decomposition of hydrates, and release of ammonia, which influences the quality of the finished product. Consequently, it is crucial to choose a fast, efficient, and economical process to reduce the overall production cost (Fang et al., 2023). The previously reported literature has studied the disintegration of struvite using calcination (Yu et al., 2013), ultrasound stripping (Huang et al., 2017), alkaline condition, acid dripping, and alkaline-microwave treatment (Chen et al., 2020). Higher temperature causes

* Corresponding author.

E-mail address: biobala@nitrkl.ac.in (P. Balasubramanian).

decomposition of the struvite crystals by releasing the structural water and ammonia from it. However, the disintegration of struvite crystals can occur in both high and low-temperature environmental conditions depending on the humidity and heating rate (Frost et al., 2004; Farhana, 2015). On the other hand, the reduction of water due to drying helps to reduce the pathogenic content in the struvite. Decrey et al. (2011) reported the inactivation of human virus surrogate $\Phi X174$ by drying due to reduction of moisture. Similarly, Bischel et al. (2016) confirmed the reduction of the *Enterococcus* spp. And *Salmonella typhimurium* inoculated during the drying of struvite. They also concluded that the decrease of microbial content has a linear relationship with the loss of moisture content as the inactivation increases at elevated temperatures. Zaffar et al. (2023) reported 99% reduction of microbes in urine during precipitation using electrocoagulation that decreases the chances of infectious occurrence in struvite. Hence, the study of the drying process using appropriate technique and condition is essential to make it an economical and efficient fertilizer.

Different methods used to reduce moisture from different waste and agricultural products are air drying, osmotic drying, solar drying, spray drying, infrared drying, drum drying, vacuum drying, conventional oven drying, freeze drying, microwave drying, foam mat drying, acoustic drying, and impingement drying (Kheto et al., 2021; Inyang et al., 2018). Conventional oven technique utilizes simple instruments with an easy and adjustable temperature control system. However, the technique offers larger air resistance, decreasing the heat transfer that affects the drying speed (Zhou et al., 2024). On the other hand, microwave oven utilizes energy conversion from microwave to heat energy that increases the temperature rapidly, enhancing the drying speed (Huang et al., 2023). High temperature exerts a large driving force on the materials, facilitating heat transfer by providing a large water-vapor deficit, helping to accelerate the drying process (Agbede et al., 2020). Thus, unraveling the mechanism behind drying is done through modelling that helps to understand the transport mechanism and influence of certain variables on moisture transfer (Inyang et al., 2017). The kinetic models help to attain desired moisture content in the operating conditions and can help to minimize the cost and energy consumption without compromising productivity or quality (Pocock et al., 2022; Wang et al., 2023).

The previous literature study is limited to the utilization of different technologies to study the struvite formation, disintegration, and the effect of different ions. Less emphasis was given to drying, which can influence the overall nutrient content and fertilizing capacity of struvite. The researchers have not explored different drying techniques to eliminate long drying hours that can help to reduce the downstream processing cost. According to the author's knowledge, no study has been reported to understand the effect of microwave power on struvite drying and the mechanism behind the different drying techniques. Hence, the present work aims at (1) a detailed study of thin layer drying of struvite produced by electrocoagulation method from source-separated urine using open sun drying, air drying, convective/hot-air oven (20–80 °C) and microwave drying (180–720 W). (2) Kinetic modelling using different drying models to comprehend the mechanism of drying. (3) To evaluate the working efficiency in terms of diffusivity constant, activation energy, specific energy and cost estimation. (4) Lastly, characterization of the precipitates using X-ray diffraction (XRD) and Fourier transformed infrared spectroscopy (FTIR) to analyze the change in the crystal structure and functional groups of struvite, respectively.

2. Materials and methods

2.1. Sample preparation

Human urine samples were collected in labeled bottles from male individuals following a healthy and regular diet. The samples were mixed and stored at –20 °C to avoid an increase in pH due to urea hydrolysis. The pH of the urine solution was maintained at 8 ± 0.3 for

struvite precipitation using 1 M NaOH and 1 M HCl. Struvite was produced by electrocoagulation using a magnesium anode on the set-up and experimental conditions, as described in the previous study by Zaffar et al. (2023). After the reaction time of 30 min, the solution was kept stable for 3 h to allow sedimentation of the precipitate at the bottom of the beaker. Decantation was followed by centrifugation to remove more than 80% of the water. The precipitate was uniformly spread up to a 3 mm thin layer over a petri plate for drying.

2.2. Drying of samples

The thin layer drying of struvite was performed utilizing air, open sun, hot air oven/convective (20–80 °C), and microwave drying (180–720 W). Open sun drying was performed by placing the petri plates directly in sunlight in the month of December at 18.6 °C average temperature, 39% humidity, and 0.1 km h⁻¹ wind speed. Air drying was carried out at 22.7 °C and 58.6% humidity at National Institute of Technology Rourkela (Latitude: 22°15'11.79" N; Longitude: 84°54'5.90"E), India. Convective drying was performed in a hot air oven (BD Instrumentation, with a cavity dimension of 450 mm [L] * 450 mm [B] * 500 mm [D]) using a temperature sensor positioned in the center and parallel hot air moving at 3.6 km h⁻¹. Similarly, microwave drying was done using a domestic microwave oven (Electrolux C25K151 BG-CG with cavity dimension 190 mm (H)* 310 mm (L) * 300 mm (W), output power 900 W, frequency 2450 Hz) with power ranging from 180 to 720 W.

The precipitate was uniformly distributed (3 mm thick) over a circular glass petri plate with a 50 mm diameter cross-sectional area. The initial mass was measured before the drying process using a weighing balance (Shimadzu digital). The instantaneous weight change was measured at 5 min intervals for the first 30 min, followed by 10 min for next 2 h, and finally, 15 min till the weight was nearly constant for solar, air, and convective drying. The change in weight for microwave drying was taken at an interval of 1 min till a constant measurement was achieved. All the experiments were done in triplicates, and the average value was reported.

2.3. Data analysis and modelling

2.3.1. Moisture ratio, drying rate, and effective diffusivity

The moisture content (X_t) in the sample (g water, g dry matter⁻¹) was evaluated using mass-time data by Eq. (1) (Pocock et al., 2022)

$$X_t = \frac{m_t - m_0}{m_0} \quad (1)$$

Where m_t is the struvite mass (g) at instantaneous time t, and m_0 is the dried mass of struvite (g)

The drying rate is calculated using Eq. (2) (Behera and Balasubramanian, 2021)

$$D_R = \frac{X_t - X_{t+dt}}{dt} \quad (2)$$

Where D_R is the drying rate (g water, g dry matter⁻¹ min⁻¹); X_{t+dt} is the moisture content (g water, g dry matter⁻¹) at time t + dt; and dt is the increment in time (min).

Utilizing the moisture content data, the dimensionless moisture ratio (M_R) was calculated using Eq. 3

$$M_R = \frac{X_t - X_e}{X_i - X_e} \quad (3)$$

where initial and equilibrium moisture content are denoted by X_i and X_e , respectively. The moisture ratio can be simplified to Eq. (4) since X_e has a low value for lengthy drying times relative to X_t and X_i (Behera and Balasubramanian, 2021)

$$M_R = \frac{X_t}{X_i} \quad (4)$$

Fick's second law of diffusion, expressed in terms of MR using Eq. (5) (Vega-Gálvez et al., 2010), governs the diffusion of moisture from the interior of the struvite to the surface layer during the time of falling rate.

$$\frac{dM_R}{dt} = D_{eff} \frac{d^2 M_R}{dx^2} \quad (5)$$

Where x is the spatial dimension (m), and D_{eff} is the effective moisture diffusivity ($\text{m}^2 \text{ s}^{-1}$). The cross-sectional area of the petri plate was round. Assuming one-dimensional transport of moisture in an infinite slab, homogeneous moisture distribution, uniform mass transfer, minimal external resistance, and shrinkage, Eq. (5) can be expressed using Eq. (6) (Crank, 1975)

$$M_R = \frac{8}{\pi^2} \sum_{i=0}^{\infty} \frac{1}{(2i+1)^2} \exp \left[\frac{-(2i+1)^2 D_{eff} \pi^2 t}{4L^2} \right] \quad (6)$$

where t is the drying period (min) and L is the half thickness (m). The first term in the series provides an accurate calculation when a longer drying interval is assumed. As a result, Eq. (6) is transformed into Eq. (7) (Di Scala and Crapiste, 2008)

$$M_R = \frac{8}{\pi^2} \exp \left[\frac{D_{eff} \pi^2 t}{4L^2} \right] \quad (7)$$

The linear representation of Eq. (7) is depicted in Eq. (8) (Agbede et al., 2020)

$$\ln(M_R) = \ln \left(\frac{8}{\pi^2} \right) - \left(\frac{D_{eff} \pi^2 t}{4L^2} \right) \quad (8)$$

The slope of the straight line created by plotting $\ln(M_R)$ versus t gives the value of D_{eff} by using Eq. (9) (Agbede et al., 2020)

$$Slope_1 = \frac{D_{eff} \pi^2}{4L^2} \quad (9)$$

2.3.2. Activation energy and specific energy

2.3.2.1. Hot air oven drying. The Arrhenius equation in Eq. (10) (Doymaz and Smail, 2011; Tunde-Akintunde and Ogunlakin, 2011) represents the relation between effective diffusivity and Arrhenius factor as a function of activation energy and temperature.

$$D_{eff} = D_0 \exp \left(\frac{E_a}{RT} \right) \quad (10)$$

Where D_0 is the Arrhenius factor ($\text{m}^2 \text{ s}^{-1}$), E_a is the activation energy (kJ mol^{-1}), R is the universal gas constant ($8.314 \text{ J mol}^{-1} \text{ K}^{-1}$), and T is the absolute temperature (K). The linear form of Eq. (10) is described in Eq. (11) (Behera and Balasubramanian, 2021).

$$\ln D_{eff} = \ln D_0 - \frac{E_a}{RT} \quad (11)$$

When $\ln D_{eff}$ vs. $1/T$ is plotted, the slope of a straight line representing the activation energy is obtained using Eq. (12) (Agbede et al., 2020)

$$Slope_2 = \frac{E_a}{R} \quad (12)$$

Eqs. 13 & 14 (Agbede et al., 2020) were used to calculate the total energy (E_t) and specific energy (E_{sp}) required for drying in a hot air oven.

$$E_t = A \nu \rho_a c_a \Delta T D_t \quad (13)$$

$$E_{sp} = \frac{E_t}{m_i - m_d} \quad (14)$$

Where A is the area of the circular petriplate (m^2) ΔT is the temperature

difference in ($^\circ\text{C}$); ν is the velocity of air (m sec^{-1}); ρ_a is the density of air (Kg m^{-3}); c_a is the specific heat capacity of air ($\text{kJ Kg}^{-1} \text{C}^{-1}$); D_t is the total drying time (s); m_i and m_d is the initial mass (g) and dried mass of the precipitate (g), respectively.

2.3.2.2. Microwave drying. The activation energy in the microwave is dependent on power, and Arrhenius's relationship between effective diffusivity and microwave power is represented in Eq. (15) (Olanipekun et al., 2015)

$$D_{eff} = D_0 \exp \left(\frac{-E_a m}{P} \right) \quad (15)$$

Where D_0 is the Arrhenius factor ($\text{m}^2 \text{ sec}^{-1}$); E_a is the activation energy (W g^{-1}); P is the microwave power (W), and m is the initial mass of struvite. By taking the natural logarithm on both sides of Eq. (15), the linear equation Eq. 16 is obtained (Behera and Balasubramanian, 2021).

$$\ln D_{eff} = \ln D_0 - \frac{E_a m}{P} \quad (16)$$

The activation energy is determined by Eq. (17) based on the slope obtained from the straight line of the plot $\ln D_{eff}$ vs m/p (Agbede et al., 2020).

$$Slope_3 = E_a \quad (17)$$

Using Eqs. 18 & 19, the total energy and the specific energy necessary for microwave drying were calculated, respectively (Agbede et al., 2020).

$$E_{t_m} = P \times D_t \quad (18)$$

$$E_{sp_m} = \frac{E_t}{m_i - m_d} \quad (19)$$

Where E_{t_m} is the total energy (kWh); P is the microwave power (kW); D_t is the drying time (h); E_{sp_m} is the specific energy (kWh kg^{-1} water removed); m_i and m_d is the initial mass (g) and dried mass of the precipitate (g), respectively.

2.3.3. Thin layer mathematical modelling of drying kinetics

Using the Origin Pro software, the experimental data of moisture ratio (MR) vs. drying time were fitted to thin-layer drying models. The twenty-two models (Table 1) have been used for curve fitting to evaluate the mechanism behind the drying data obtained from struvite drying experiments. To determine the optimum fit, statistical parameters such as the adjusted coefficient of determination (R^2), reduced chi-square (χ^2), root mean square error (RMSE), and sum of square error (SSE) are used. The model having the highest R^2 and lowest values of χ^2 , RMSE, and SSE best describes the experimental data. Using Eqs. (20)–(22), the values SSE, RMSE, and χ^2 were calculated from Origin Pro (2022); Behera and Balasubramanian (2021).

$$SSE = \frac{1}{N} \sum_{i=1}^N (M_{R_{exp,i}} - M_{R_{pred,i}})^2 \quad (20)$$

$$RMSE = \left[\frac{1}{N} \sum_{i=1}^N (M_{R_{exp,i}} - M_{R_{pred,i}})^2 \right]^{\frac{1}{2}} \quad (21)$$

$$\chi^2 = \frac{\sum_{i=1}^N (M_{R_{exp,i}} - M_{R_{pred,i}})^2}{N - z} \quad (22)$$

Where N is the number of observations; z is the number of constants. $M_{R_{exp,i}}$ and $M_{R_{pred,i}}$ stands for the experimental and predicted moisture ratios, respectively.

Table 1

Thin layer models for mathematical modelling of drying data of struvite.

No	Model Name	Model Equation	References
1	Newton	$M_R = \exp(-kt)$	Westerman et al. (1973)
2	Page	$M_R = \exp(-kt^n)$	Page, (1949)
3	Modified Page	$M_R = \exp[(-kt)^n]$	Yaldýz and Ertekýn (2001)
4	Modified Page II	$M_R = \exp\left[-k\left(\frac{t}{L^2}\right)^n\right]$	Midilli et al. (2002)
5	Modified Page III	< ! – Q5 : The citation(s) '1 = 63700 = = = Kumar et al., 2006' has/have been changed to match the author name/date in the reference list. Please check here and in subsequent occurrences, and correct if necessary. – – > $M_R = k \exp\left(-\frac{t}{d^2}\right)^n$	Praveen Kumar et al., (2006)
6	Henderson and Pabis	$M_R = a \exp(-kt)$	Behera and Balasubramanian (2021)
7	Logarithmic	$M_R = a \exp(-kt) + c$	Yaldýz and Ertekýn (2001)
8	Two term	$M_R = a \exp(-k_0 t) + b \exp(-k_1 t)$	Rahman et al. (1997)
9	Two term exponential	$M_R = a \exp(-kt) + (1-a) \exp(kat)$	(Yaldiz et al., 2001)
10	Wang and Singh	$M_R = 1 + at + bt^2$	Agbede et al. (2020)
11	Singh et al.	$M_R = \exp(-kt) - akt$	Inyang et al. (2018)
12	Approximation of Diffusion	$M_R = a \exp(-kt) + (1-a)\exp(-kbt)$	Yaldýz and Ertekýn (2001)
13	Verma et al.	$M_R = a \exp(-kt) + (1-a)\exp(-gbt)$	Verma et al. (1985)
14	Modified Handerson and Pabis	$M_R = a \exp(-kt) + b \exp(-gt) + c \exp(-ht)$	Inyang et al. (2018)
15	Aghabashlo	$M_R = \exp\left(-\frac{k_1 t}{1+k_0 t}\right)$	Inyang et al. (2018)
16	Ademiluyi Modified	$M_R = a \exp(-kt)^n$	Ademiluyi et al. (2008)
17	Weibull	$M_R = \exp\left(-\left(\frac{t}{a}\right)^b\right)$	Corzo et al. (2008)
18	Midilli et al.	$M_R = a \exp(-kt^n) + bt$	Midilli et al. (2002)
19	Silva et al.	$M_R = \exp\left(-at - \frac{1}{bt^2}\right)$	Silva et al. (2012)
20	Combined two term and page	$M_R = a \exp(-kt^n) + b \exp(-ht^n)$	Hii et al. (2008)
21	Hasibuan and Daud	$M_R = 1 - at^n \exp(-kt^n)$	Ertekin and Heybeli (2014)
22	Simplified ficks diffusion	$M_R = a \exp(-kt) + c$	Celma et al. (2007)

2.4. Characterization of the struvite precipitate

The dried samples were analyzed using attenuated total reflectance of Fourier transformed infrared spectroscopy (ATR, FTIR) (Bruker Alpha E) at a scan rate of 400–4000 cm⁻¹ to evaluate the change in functional group and quality of struvite. Further, the precipitate was analyzed using X-Ray diffraction (XRD) (Empyrean: Multi-functional X-Ray Diffraction System, Malvern Panalytical) from 2θ range of 10–70° at a scan rate of 6° min⁻¹ with 0.02 step size to comprehend the effect of drying on the crystal structure.

3. Results and discussion

3.1. Drying characteristics

3.1.1. Open sun and air-drying

The plot between moisture ratio and drying time implies that moisture levels get lower with time under both open-air and air-drying settings (Fig. 1 (a, b)). The energy of the sun and wind was utilized for moisture removal in open sun conditions. On the other hand, at room temperature, a portion of water molecules evaporate by utilizing their energy to break with other water molecules. The drying time for sun and air drying is 6 h and 30 h, respectively. The thermal heating by solar radiation in the presence of wind and lower humidity enhanced moisture reduction, decreasing the time taken for drying. On the contrary, the absence of any external energy to heat up the precipitate and high humidity caused an increase in drying time in room conditions (Masmoudi et al., 2021). Somorin et al. (2020) also reported a five-fold increase in drying time in the case of non-isothermal drying of feces.

In the open sun, a faster drying rate was observed during the initial

period, which slowed down with time, whereas an overall slow drying rate was concluded from air drying (Fig. 1 c). The constant decrease in drying rate implies that the drying of the precipitate in both conditions was dependent on moisture diffusion from the inner layer to the surface. Similar results were observed for open sun drying of wastewater municipal sludge (Ameri et al., 2020; Masmoudi et al., 2021), sanitation products (Pocock et al., 2022), algae (Agbede et al., 2020). Besides, due to the prolonged drying time caused by the high humidity in the air, the drying rate was reduced in air drying. The influence of high humidity is attributed to a decrease in the moisture gradient between the precipitate and the surrounding air, decreasing the mass transfer, which eventually affects the drying rate (Pocock et al., 2022).

The parameters used for the calculation of effective diffusivity under different drying conditions are summarized in Table 2. The effective diffusivity of $1.36 \times 10^{-8} \pm 7.04 \times 10^{-10}$ m² s⁻¹ and $2.16 \times 10^{-9} \pm 1.26 \times 10^{-10}$ m² s⁻¹ was observed for sun and room drying, respectively. The higher moisture diffusivity of sun drying confirms the results reported above. The effective diffusivity was found to be of similar order as obtained from direct and indirect solar drying of municipal sludge (Ameri et al., 2020). The effective diffusivity reported by (Wang et al., 2019) for rooftop drying of sewage sludge with variable solar radiation is lower than the measured diffusivity for both situations. The results conclude that struvite has a similar or higher magnitude of effective diffusivities as sewage sludge.

3.1.2. Hot air drying

The plot of varying moisture ratio versus time with changing temperature (20–80 °C) is illustrated in Fig. 2a. The moisture content of struvite (3 mm thickness spread in petri plates) decreases over time at all temperatures. The time of moisture removal decreased with the increase

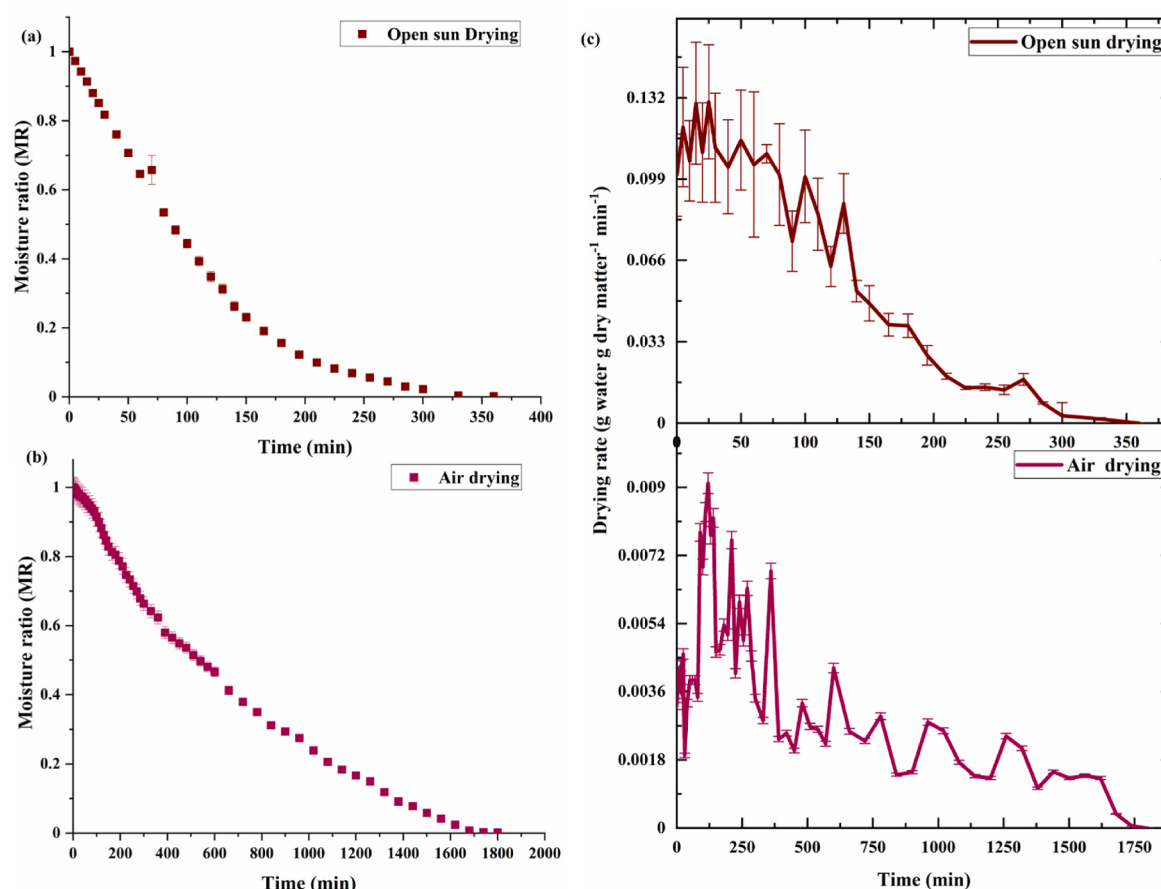


Fig. 1. (a,b) Effect of open sun drying and air drying on moisture ratio of precipitate with time; (c) Drying rate curve of struvite at different drying conditions.

Table 2

Diffusion data of struvite drying at different conditions.

Drying Condition	Slope	Effective Diffusivity ($\text{m}^2 \text{s}^{-1}$)	R^2
Open sun Drying	$-0.01 \pm 7.71\text{E-}4$	1.36E-08	0.93
Air Drying	$-0.002 \pm 1.38\text{E-}4$	2.16E-09	0.84
Convective Drying 20 °C	$-0.003 \pm 1.36\text{E-}4$	2.53E-09	0.89
Convective Drying 40 °C	$-0.008 \pm 2.58\text{E-}4$	7.11E-09	0.97
Convective Drying 60 °C	-0.02 ± 0.002	2.05E-08	0.86
Convective Drying 80 °C	-0.06 ± 0.005	5.40E-08	0.92
Microwave Drying 180 W	-0.06 ± 0.002	5.77E-08	0.94
Microwave Drying 360 W	-0.15 ± 0.007	1.35E-07	0.94
Microwave Drying 540 W	-0.19 ± 0.01	1.74E-07	0.93
Microwave Drying 720 W	-0.48 ± 0.04	4.36E-07	0.92

of temperature, as the air is heated at a faster rate in a non-humid condition. Further, the decline in the moisture ratio indicated an increase in the drying process, where the drying time decreased at higher temperatures. The decline in drying time from 24 h at 20 °C to 8 h at 40 °C was observed, followed by further reduction to 3.5 h and 90 min when the temperature increased to 60 °C and 80 °C, respectively (Fig. 2b). Higher temperatures enhance water activity, which accelerates drying in a shorter amount of time due to the rise in heat energy (Agbede et al., 2020). A similar conclusion was reported by Pocock et al. (2022) for convective drying of fecal sludge from ventilated improved pit toilets. Further, the decline in drying rate was observed with time for all the drying temperatures. The falling rate is the influence of internal mass and heat transfer. The increase in air temperature increases the temperature gradient between the material and the surroundings, speeding up the mobility of moisture, resulting in higher heat and mass transfer, further enhancing the heat available for evaporation

of the moisture. Additionally, the removal of internal water increases the pore volume and surface area, enhancing the drying process at higher temperatures (Huang and Chen, 2017).

The influence of temperature on mass transfer was clarified by calculating the effective diffusivity of struvite drying at all temperatures. The diffusivity of the sample increased by increasing the temperature from 20 to 80 °C. It varied from $2.53 \times 10^{-9} \pm 1.24 \times 10^{-10}$ at 20 °C to $5.40 \times 10^{-8} \pm 4.94 \times 10^{-9} \text{ m}^2 \text{s}^{-1}$ at 80 °C. The increase in diffusivity with temperature indicates the enhancement of moisture removal from the sample as the pore structure collapses, leading to an increase in permeability (Huang and Chen, 2017). The values of similar magnitude were reported by Pocock et al. (2022) for the drying of fecal sludge. The diffusivity was much higher than that stated by Zhang et al. (2016) for sewage sludge/lignite briquettes with temperatures varying from 60 to 180 °C. The measured activation energy is 43.97 kJ mol⁻¹, which should be overcome by a hot air oven for the drying process. The activation energy was higher than that reported for convective drying of municipal sludge from 100 to 160 °C by Huang et al. (2017). Similarly, Somorin et al. (2020) have concluded the activation energy of anaerobic baffle reactor, human feces, urine-diverting dry toilet and ventilated improved pits to be 34 ± 0.8 kJ mol⁻¹, 30.5 ± 0.1 kJ mol⁻¹, 28.3 ± 1.3 kJ mol⁻¹, 36 ± 0.3 kJ mol⁻¹ drying between the temperature of 65–205 °C. The use of a higher temperature than the present study might be the reason of such discrepancy in the activation energy.

3.1.3. Microwave drying

Fig. 3a depicts the relationship between moisture ratio and drying time for microwave powers between 180 and 720 W. The decrease of moisture ratio with time implied successful removal of moisture as the drying process progressed. The removal of moisture from struvite increased at higher microwave power, resulting in a shorter drying time. The drying time decreased from 52 ± 2 min at 180 W to 12 ± 2 min at 720 W. High power produces high microwave energy, which consequently increases the heat energy due to the frictional movement of dipole leading to rapid evaporation of water from the sample (Agbede et al., 2020). Further, shorter drying time has been observed in

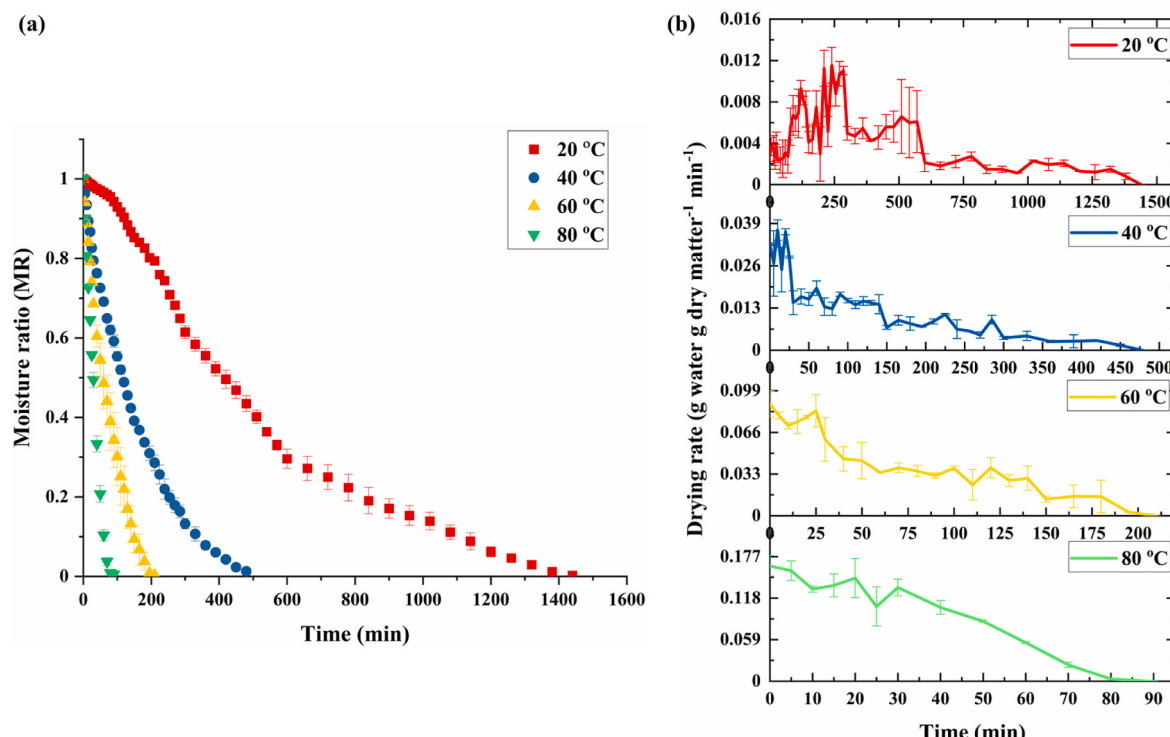


Fig. 2. Effect of convective heating temperatures (20–80 °C) on (a) moisture ratio and (b) drying rate of precipitate at different temperatures.

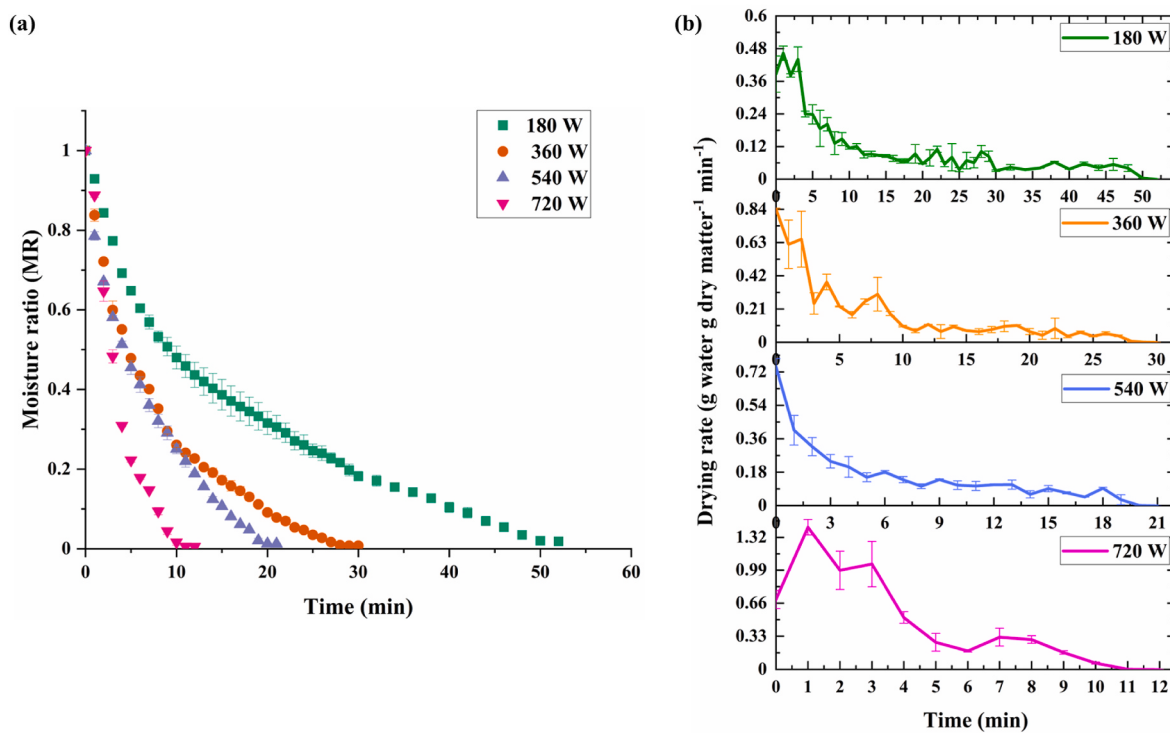


Fig. 3. Effect of microwave powers (180–720 W) on (a) moisture ratio and (b) drying rate of precipitate at different power.

microwaves as compared to convective, open sun, and air drying. Microwave radiation ensures uniform and improvised heating increases the temperature of surrounding air rapidly, thereby enhancing the process of moisture removal as compared to other techniques (Behera and Balasubramanian, 2021; Wulyapash et al., 2022). Previous literature reports a similar conclusion for the drying of sewage sludge (Chen et al., 2020), chromium-rich electroplating sludge (Zhang et al., 2023), hydrocarbon cutting sludge (Tinmaz Köse et al., 2019) at different microwave power.

The confirmation of no or shorter initial warm-up or initiation phase in the drying curve further signified the faster removal of moisture from struvite under the effect of microwave radiation as compared to other techniques (Fig. 3b). Water molecules dominate the microwave absorptivity on the precipitate, resulting in the rapid removal of water under the influence of the microwave. Additionally, as moisture ratios drop, the penetration of microwave radiation rises due to a fall in the dielectric loss angle tangent (Zhang et al., 2023). Wulyapash et al. (2022) reported comparable outcomes for drying dewatered sludge using microwave power ranging from 100 W to 800 W.

The effective diffusivity at 180 W, 360 W, 540 W, and 720 W are $5.77 \times 10^{-8} \pm 2.23 \times 10^{-9} \text{ m}^2 \text{ s}^{-1}$; $1.35 \times 10^{-7} \pm 6.51 \times 10^{-9} \text{ m}^2 \text{ s}^{-1}$; $1.74 \times 10^{-7} \pm 1.10 \times 10^{-8} \text{ m}^2 \text{ s}^{-1}$ and $4.36 \times 10^{-7} \pm 3.99 \times 10^{-8} \text{ m}^2 \text{ s}^{-1}$, respectively. Bennamoun et al. (2014) have reported a similar range of effective diffusivity for drying wastewater sludge at different microwave power. Zhang et al. (2021) have also observed a similar magnitude of effective diffusivity for drying paper towel waste. The uniform and volumetric heating produced by microwave radiation increases the temperature, intensifying diffusion. Thus, power is the most influential parameter for microwave drying, whose enhancement increases the diffusion coefficient of the precipitate (Bennamoun et al., 2014). Additionally, the minimum energy required to start moisture diffusion from the interior to the exterior of struvite during microwave drying is 54.14 W kg^{-1} . The activation energy is lower than the previously reported microwave drying study on the combination of fecal and urine samples for 20 g, 30 g, and 40 g, were 20.37 W g^{-1} , 14.95 W g^{-1} , and 11.28 W g^{-1} , respectively (Ganesa Pillai et al., 2022) as the effective

diffusivity is higher in the present study that has led to the decrease of activation energy.

3.2. Mathematical modelling of drying kinetics

3.2.1. Open sun and air-drying

Table 3 illustrates the curve fitting and statistical inference of the drying data. The models having the adjusted coefficient correlation equivalent or more than 0.95 with low RMSE are a better fit than others. In open sun drying, many models have shown best fitting with the adjusted R^2 value of 0.99. However, Ademiluyi modification was concluded as the best fit with adjusted R^2 (0.99) and lowest χ^2 , RMSE, and SSE values of 2.23E-4, 0.01, and 0.01, respectively. The other models that showed best fitting were Page, Modified Page, Wang and Singh, Singh et al., Hasibuan and Daud, and Simplified Ficks diffusion having the adjusted correlation coefficient values of 0.99 with RMSE values between 0.02–0.03. Previous scientific studies have reported similar models to be suitable for drying ghost pepper (Rabha et al., 2017); apple slices (Noori et al., 2021), and algae (Agbede et al., 2020) in open sun. In the case of air drying, fewer models had the coefficient of correlation substantial to the best fit. The Simplified Ficks diffusion had R^2 equivalent to 0.99 with the lowest RMSE value of 0.01 among all the selected models, making it appropriate to comprehend the mechanism for air drying.

3.2.2. Hot air drying

The modelling and the statistical parameters for convective drying at varying temperatures are reported in Table 4. The Verma et al., Hasibuan, and Daud and simplified Ficks diffusion have shown the best fit among the nine models with the R^2 value of 0.99. However, the Verma et al. model has the lowest χ^2 , RMSE, and SSE values of 1.97E-4, 0.01, and 0.01 at 20 °C. On the other hand, except Wang and Singh, all the other twelve models had a correlation coefficient of 0.99 at 40 °C, with Simplified Ficks diffusion model having 0.003 as the lowest RMSE. When the temperature was further increased to 60 °C and 80 °C, many models showed the best-fit characteristic, but the lowest RMSE was

Table 3

Kinetic modelling and statistical parameters for open sun and air drying of struvite.

	Model	Parameter	R ²	χ^2	RMSE	SSE
Open sun Drying	Newton	k = 0.01 ± 2.84E-4	0.98	0.002	0.05	0.07
	Page	k = 0.002 ± 2.56E-4	0.99	2.79E-4	0.02	0.01
		n = 1.30 ± 0.03				
	Modified Page	k = 0.01 ± 8.33E-5	0.99	2.79E-4	0.02	0.01
		n = 1.31 ± 0.02				
	Modified Page III	k = 1.06 ± 0.02	0.98	0.001	0.04	0.04
		d = 1.84 ± 5.66				
		n = 0.03 ± 0.20				
	Henderson and Pabis	a = 1.06 ± 0.02	0.98	0.001	0.04	0.05
		k = 0.01 ± 3.22E-4				
	Wang and Singh	a = -0.01 ± 7.43E-5	0.99	4.30E-4	0.02	0.01
		b = 1.09E-5 ± 2.78E-7				
Air drying	Singh et al.	a = 0.01 ± 6.67E-4	0.99	4.55E-4	0.02	0.45
		k = 0.01 ± 3.44E-5				
	Approximation of Diffusion	a = 1.00 ± 0.00	0.98	0.003	0.05	0.06
		b = 1.00 ± 0.00				
		k = 0.01 ± 2.94E-4				
	Ademiluyi Modified	a = 0.98 ± 0.01	0.99	2.23E-4	0.01	0.01
		k = 0.01 ± 1.00E-4				
		n = 1.38 ± 0.03				
	Hasibuan and Daud	a = 0.004 ± 3.97E-4	0.99	2.53E-4	0.02	0.01
		k = 0.001 ± 1.48E-4				
		n = 1.13 ± 0.02				
	Simplified ficks diffusion	a = 1.16 ± 0.02	0.99	7.29E-4	0.03	0.02
		k = 0.01 ± 3.89E-4				
		c = -0.12 ± 0.02				
Air drying	Newton	k = 0.001 ± 2.55E-5	0.98	0.001	0.04	0.07
	Modified Page III	k = 1.04 ± 0.01	0.99	8.89E-4	0.03	0.05
		d = 2.08 ± 3.83				
		n = 0.01 ± 0.02				
	Henderson and Pabis	a = 1.04 ± 0.01	0.99	8.73E-4	0.03	0.05
		k = 0.001 ± 2.82E-5				
	Two term exponential	a = 1.68 ± 0.029	0.99	5.13E-4	0.02	0.03
		k = 0.002 ± 4.46E-5				
	Wang and Singh	a = -0.001 ± 1.24E-5	0.99	4.51E-4	0.02	0.03
		b = 3.02E-7 ± 8.90E-9				
	Singh et al.	a = 0.07 ± 0.01	0.99	2.08E-4	0.01	0.01
		k = 0.001 ± 1.73E-5				
Air drying	Simplified ficks diffusion	a = 1.18 ± 0.013	0.99	1.73E-4	0.01	0.01
		k = 0.001 ± 2.71E-5				
		c = -0.17 ± 0.01				

observed by Hasibuan and Daud models, having values of 0.011 and 0.01, respectively. Overall, Hasibuan and Daud was the best model describing the drying data, suggesting a correlation between the average moisture content and drying time, followed by simplified Fick's diffusion model. The literature accounts for no research reporting the use of these models for convective drying of struvite or related products. It deals with the explanation of the drying curve with better curve fitting but imparts little knowledge about the drying process (Inyang et al., 2018). The second-best fit is a semi-empirical/theoretical model created from Newton's rule of cooling and Fick's second law of diffusion by its modification. The study of Pocock et al. (2022) reported the Page model as the close fit model for convective drying fecal matter from ventilated improved pit latrines from 40 °C to 80 °C that follows the same law as simplified Fick's diffusion to explain the mechanism of drying. Similarly, Huang et al. (2017) has also reported the Modified Page model for drying mechanism as the best-fit model for sewage sludge. Convective drying is dependent on airspeed, temperature, and material thickness for efficient moisture dispersion. The increment in the constant k of Henderson and Pabis model agrees with the enhancement of effective diffusivity with the rise in temperature, making the drying process more efficient (Behera and Balasubramanian, 2021). Thus, the above-reported results were corroborated further.

3.2.3. Microwave drying

The results of fitting the drying curve and its statistical validation for microwave drying of struvite between 180 and 720 W are summarized in Table 5. The models having the R² value between 0.95 and 0.99 with the

lowest χ^2 , RMSE, and SSE values are considered as best fit. The microwave drying at 180 W showed a maximum correlation coefficient value of 0.99 for Page, Modified Page, Ademiluyi modified, Modified Henderson, and Pabis and Weibull models. However, the lowest statistical parameters, such as χ^2 (2.55E-4), RMSE (0.015), and SSE (0.009), correspond to the Weibull model at 180 W. Further increasing the power to 360 W, Weibull and Midilli et al. reported the highest R² value with the lowest RMSE value of 0.006. The increase of power to 540 W concluded simplified Fick's diffusion as the best fit, followed by Hasibuan and Daud, and Weibull, which corresponded to the lowest RMSE values of 0.003, 0.004, and 0.006, respectively. Similarly, Page, Modified Page, Modified Page III, Two-term exponential, Verma et al., Weibull, and combined two-term and Page had the highest correlation of coefficient value at 720 W, but combined two-term and Page model concluded the lowest RMSE (0.017). Overall, the Weibull model shows a consistent fitting of drying data with the lowest statistical parameters as compared to other models. According to the author's knowledge, the literature reports no data corresponding to this model for microwave drying. The Weibull models belong to the empirical category, which provides good data fitting and is independent of the features of the material that is dried (Horuz et al., 2017). Likewise, an empirical model was reported to be the best fit for microwave drying of the Mabonde banana variety (Omolola et al., 2014). Thus, Weibull is the best-fit model for microwave drying of struvite produced by source-separated urine.

Table 4

Kinetic modelling and statistical parameters for hot air oven drying of struvite at varying temperatures (20 °C–80 °C).

Model		Parameter	R ²	χ^2	RMSE	SSE
20 °C	Newton	k = 0.002 ± 5.37E-5	0.97	0.003	0.06	0.18
	Modified Page III	k = 1.08 ± 0.01 d = 1.88 ± 5.06 n = 0.01 ± 0.04	0.98	0.002	0.04	0.09
Henderson and Pabis		a = 1.08 ± 0.01 k = 0.002 ± 5.27E-5	0.98	0.002	0.04	0.09
		a = -0.001 ± 2.67E-5 b = 4.56E-7 ± 2.42E-8	0.98	0.001	0.04	0.07
Wang and Singh		a = 0.10 ± 0.02 k = 0.001 ± 6.53E-5	0.98	0.001	0.04	0.10
		a = -0.44 ± 0.07 k = 0.01 ± 9.40E-4 g = 0.002 ± 8.15E-5	0.99	1.97E-4	0.01	0.01
Singh et al.		a = 3.36E-4 ± 5.72E-5 k = 1.29E-4 ± 2.23E-5 n = 1.24 ± 0.03	0.99	5.91E-4	0.02	0.03
		a = 1.23 ± 0.03 k = 0.001 ± 7.88E-5 c = -0.17 ± 0.03	0.99	9.34E-4	0.03	0.04
Verma et al.		a = 0.01 ± 7.16E-5 n = 1.02 ± 0.02	0.99	3.43E-4	0.02	0.01
		a = 0.01 ± 5.63E-4 n = 1.02 ± 0.02	0.99	3.40E-4	0.02	0.01
Hasibuan and Daud		a = 0.01 ± 7.04E-5 n = 1.02 ± 0.02	0.99	3.40E-4	0.02	0.01
		a = 0.10 ± 0.01 d = 2.20 ± 3.35 n = 0.03 ± 0.09	0.99	3.53E-4	0.02	0.01
40 °C	Newton	k = 0.01 ± 7.16E-5	0.99	3.43E-4	0.02	0.01
	Page	k = 0.01 ± 5.63E-4 n = 1.02 ± 0.02	0.99	3.40E-4	0.02	0.01
Modified Page		k = 0.01 ± 7.04E-5 n = 1.02 ± 0.02	0.99	3.40E-4	0.02	0.01
		k = 0.10 ± 0.01 d = 2.20 ± 3.35 n = 0.03 ± 0.09	0.99	3.53E-4	0.02	0.01
Modified Page III		k = 0.01 ± 9.45E-5 a = 0.99 ± 0.01	0.99	3.42E-4	0.02	0.01
		a = 1.42 ± 0.07 k = 0.01 ± 2.92E-4	0.99	3.01E-4	0.02	0.01
Henderson and Pabis		a = -0.004 ± 8.80E-5 b = 5.93E-6 ± 2.47E-7	0.98	0.001	0.04	0.04
		a = 0.02 ± 0.003 k = 0.01 ± 7.91E-5	0.99	1.75E-4	0.01	0.01
Two term exponential		a = -0.004 ± 8.80E-5 b = 5.93E-6 ± 2.47E-7	0.98	0.001	0.04	0.04
		a = 0.02 ± 0.003 k = 0.01 ± 7.91E-5	0.99	1.75E-4	0.01	0.01
Wang and Singh		a = 0.02 ± 0.003 k = 0.01 ± 7.91E-5	0.99	1.75E-4	0.01	0.01
		a = 0.02 ± 0.003 k = 0.01 ± 7.91E-5	0.99	1.75E-4	0.01	0.01
Singh et al.		a = 0.02 ± 0.003 k = 0.01 ± 7.91E-5	0.99	1.75E-4	0.01	0.01
		a = -3.60E10 ± 2.28E11	0.99	2.20E-4	0.01	0.01

Table 4 (continued)

Model	Parameter	R ²	χ^2	RMSE	SSE
Ademiluyi Modified	b = 1.00 ± 7.38E-11 k = 0.004 ± 2.06E-4 a = 0.97 ± 0.01 k = 0.01 ± 8.80E-5 n = 1.09 ± 0.03	0.99	2.60E-4	0.02	0.01
	Hasibuan and Daud	a = 0.01 ± 4.83E-4 k = 0.003 ± 1.55E-4 n = 0.87 ± 0.01	0.99	6.30E-5	0.01
Simplified ficks diffusion	a = 1.05 ± 5.21E-4 k = 0.01 ± 8.10E-6 c = -0.08 ± 6.08E-4	0.99	1.29E-5	0.003	0.01
	Newton	k = 0.01 ± 3.35E-4	0.98	0.001	0.03
Page	k = 0.01 ± 0.001 n = 1.12 ± 0.04	0.99	7.52E-4	0.03	0.02
	Modified Page	k = 0.01 ± 2.48E-4 n = 1.12 ± 0.04	0.99	7.52E-4	0.03
Modified Page III	k = 1.02 ± 0.02 d = 1.98 ± 6.48 n = 0.05 ± 0.34	0.98	0.001	0.03	0.02
	Henderson and Pabis	k = 0.01 ± 4.36E-4 a = 1.02 ± 0.02	0.98	0.001	0.02
Two term exponential	a = 1.62 ± 0.07 k = 0.02 ± 7.29E-4	0.99	7.06E-4	0.03	0.01
	Wang and Singh	a = -0.01 ± 1.74E-4 b = 2.36E-5 ± 1.08E-6	0.99	6.18E-4	0.02
Singh et al.	a = 0.05 ± 0.01 k = 0.01 ± 1.94E-4	0.99	1.46E-4	0.01	0.003
	Ademiluyi Modified	a = 0.97 ± 0.02 k = 0.01 ± 3.45E-4 n = 1.19 ± 0.06	0.99	6.99E-4	0.03
Hasibuan and Daud	a = 0.02 ± 0.001 k = 0.01 ± 3.12E-4 n = 0.91 ± 0.02	0.99	1.18E-4	0.01	0.002
	Simplified ficks diffusion	a = 1.16 ± 0.02 k = 0.01 ± 3.43E-4 c = -0.18 ± 0.02	0.99	1.50E-4	0.01
Newton	k = 0.03 ± 0.002 k = 0.01 ± 0.002	0.96	0.005	0.07	0.05
	Page	k = 0.01 ± 0.002 k = 0.01 ± 0.002	0.99	8.31E-4	0.03

(continued on next page)

Table 4 (continued)

Model	Parameter	R ²	χ^2	RMSE	SSE
Modified Page	n = 1.41 ± 0.07 k = 0.03 ± 6.67E-4	0.99	8.31E-4	0.03	0.01
Modified Page III	n = 1.41 ± 0.07 k = 1.07 ± 0.05 d = 1.75 ± 13.01 n = 0.09 ± 1.39	0.96	0.004	0.07	0.04
Henderson and Pabis	k = 0.03 ± 0.002 a = 1.07 ± 0.05	0.96	0.004	0.06	0.04
Two term exponential	a = 1.90 ± 0.07 k = 0.04 ± 0.002	0.99	0.001	0.04	0.01
Wang and Singh	a = -0.02 ± 3.75E-4 b = 1.05E-4 ± 5.18E-6	0.99	3.09E-4	0.02	0.003
Singh et al.	a = 0.12 ± 0.03 k = 0.02 ± 0.001	0.99	0.001	0.03	0.01
Ademiluyi Modified	a = 0.96 ± 0.02 k = 0.03 ± 7.65E-4 n = 1.52 ± 0.09	0.99	6.92E-4	0.03	0.01
Hasibuan and Daud	a = 0.01 ± 7.43E-5 k = 0.003 ± 2.78E-5 n = 1.25 ± 0.002	0.99	5.33E-5	0.01	0.05
Simplified ficks diffusion	a = 1.25 ± 0.004 k = 0.02 ± 2.47E-4 c = -0.19 ± 0.01	0.99	6.37E-4	0.03	0.63

3.3. Energy requirement for struvite drying

The energy requirement for drying of struvite crystals at different temperatures for convective drying is represented in Fig. 4a. The decrease of the specific energy from $165.55 \pm 5.61 \text{ kWh kg}^{-1}$ water at 20°C to $128.59 \pm 3.05 \text{ kWh kg}^{-1}$ water at 40°C followed by further decrease to $76.11 \pm 2.56 \text{ kWh kg}^{-1}$ water and $48.05 \pm 1.16 \text{ kWh kg}^{-1}$ water when the temperature was elevated to 60°C and 80°C , respectively. The result implies that the energy required for drying decreases at higher temperatures due to an increase in drying rates and reduced drying time. The study conducted by Dhurve et al. (2022) for hot air drying between 40 and 60°C has reported a higher specific energy consumption (SEC) of $524.09 \text{ kWh kg}^{-1}$ for watermelon seeds. Similarly, for microwave drying, a reduction of SEC was observed from $30.50 \pm 0.85 \text{ kWh kg}^{-1}$ water to $23.06 \pm 0.69 \text{ kWh kg}^{-1}$ water at 180 W and 720 W , respectively (Fig. 4b). The calculated SEC is much higher than the previously reported study on microwave drying of sewage sludge with a power range of 2 kW – 6 kW (Guo et al., 2021). High microwave power usage shortens the drying process, which may account for a decrease in specific energy consumption reported in the previous literature. Besides power, the sample load also affects energy consumption. The energy requirement is more for drying lighter samples than for heavier ones (Ganesa Pillai et al., 2022).

The cost of convective drying was observed to be 13.90 – 4.03 USD for different temperature ranges (20 – 80°C), assuming the cost of 1 kWh of

Table 5

Kinetic modelling and statistical parameters for microwave drying of struvite from 180 W to 720 W .						
	Model	Parameter	R ²	χ^2	RMSE	SSE
180 W	Newton	k = 0.06 ± 0.001	0.97	0.002	0.04	0.07
	Page	k = 0.11 ± 0.01 n = 0.81 ± 0.02	0.99	5.24E-4	0.02	0.02
	Modified Page	k = 0.06 ± 9.52E-4 n = 0.81 ± 0.012	0.99	5.24E-4	0.02	0.02
	Modified Page III	k = 0.91 ± 0.02 d = 2688.50 ± 6908.80 n = 406,378.04 ± 2,097,240.40	0.98	0.001	0.03	0.04
	Henderson and Pabis	k = 0.06 ± 0.001 a = 0.91 ± 0.015	0.98	0.001	0.03	0.04
	Two term exponential	a = 0.10 ± 651,438.05 k = 0.06 ± 68.01	0.97	0.002	0.04	0.07
	Singh et al.	a = -0.01 ± 0.004 k = 0.07 ± 0.002	0.97	0.002	0.04	0.06
	Modified Handerson and Pabis	a = 0.12 ± 0.01 b = 0.22 ± 0.06 c = 0.68 ± 0.05 k = 0.05 ± 0.003 g = 0.38 ± 0.14 h = 0.049 ± 0.002	0.99	3.65E-4	0.02	0.01
	Ademiluyi Modified	a = 0.10 ± 0.02 k = 0.06 ± 0.002 n = 0.80 ± 0.03 a = -0.23 ± 0.06 b = -1.26 ± 0.07 k = 0.12 ± 0.01 n = 0.65 ± 0.03	0.99	5.38E-4	0.02	0.02
	Weibull	a = -0.23 ± 0.06 b = -1.26 ± 0.07 k = 0.12 ± 0.01 n = 0.65 ± 0.03	0.99	2.55E-4	0.015	0.01
360 W	Newton	k = 0.13 ± 0.002	0.98	7.605E-4	0.03	0.02
	Page	k = 0.18 ± 0.01 n = 0.87 ± 0.02	0.99	2.87E-4	0.02	0.01
	Modified Page	k = 0.13 ± 9.59E-5 n = 1.02 ± 0.001	0.99	3.31E-5	0.01	0.03
	Modified Page III	k = 0.94 ± 0.017	0.99	5.16E-4	0.02	0.01

(continued on next page)

Table 5 (continued)

Model	Parameter	R ²	χ^2	RMSE	SSE
	d = 2986.40 ± 5258.60				
	n = 1,101,136.29 ± 3,901,173.48				
Henderson and Pabis	k = 0.12 ± 0.002 a = 0.94 ± 0.01	0.99	4.98E-4	0.02	0.01
Two term exponential	a = 1.32 ± 0.01 k = 0.14 ± 4.37E-4	0.99	3.17E-5	0.01	0.03
Approximation of Diffusion	a = -1.46 ± 7.84E11 b = 1.00 ± 1.38E-16 k = 0.11 ± 5.13E-4	0.98	7.90E-4	0.03	0.02
Ademiluyi Modified	a = 0.99 ± 0.02 k = 0.13 ± 0.003 n = 0.88 ± 0.02	0.99	2.94E-4	0.02	0.01
Weibull	a = -0.004 ± 7.37E-4 b = -0.99 ± 0.002 k = 0.12 ± 8.866E-4 n = 1.01 ± 0.003	0.99	3.12E-5	0.006	0.03
Midilli et al.	a = 1.00 ± 0.001 b = -1.11E-4 ± 2.15E-5 k = 0.12 ± 8.84E-4 n = 1.02 ± 0.002	0.99	3.13E-5	0.006	0.03
Hasibuan and Daud	a = 0.21 ± 0.01 k = 0.08 ± 0.002 n = 0.70 ± 0.02	0.99	1.71E-4	0.01	0.004
Simplified ficks diffusion	a = 0.94 ± 0.02 k = 0.12647 ± 0.01 c = 0.01 ± 0.01	0.99	5.09E-4	0.02	0.01
540 W	Newton	k = 0.15 ± 0.004	0.98	0.001	0.03
	Page	k = 0.19 ± 0.01 n = 0.90 ± 0.04	0.98	8.41E-4	0.03
	Modified Page	k = 0.16 ± 0.004 n = 0.90 ± 0.03	0.98	8.41E-4	0.03
	Modified Page III	k = 0.95 ± 0.02 d = 11.89 ± 33.18 n = 20.40 ± 114.42	0.98	8.59E-4	0.03
Henderson and Pabis	k = 0.14 ± 0.004 a = 0.95 ± 0.02	0.98	8.16E-4	0.03	0.02
Two term exponential	a = 0.51 ± 0.12	0.98	0.001	0.03	0.02

Table 5 (continued)

Model	Parameter	R ²	χ^2	RMSE	SSE
	k = 0.22 ± 0.05				
Singh et al.	a = 0.003 ± 0.01 k = 0.15 ± 0.01	0.98	0.001	0.03	0.02
Approximation of Diffusion	a = 4.02E-11 ± 1.18E-11 b = 1.00 ± 4.59E-13	0.98	7.50E-4	0.02	0.32
Verma et al.	k = 0.15 ± 0.03 a = 0.90 ± 0.02 k = 0.14 ± 0.004 g = 122.67 ± 0.001	0.99	5.78E-4	0.02	0.01
Ademiluyi Modified	a = 0.9 ± 0.02 k = 0.15 ± 0.01 n = 0.95 ± 0.05	0.98	8.15E-4	0.03	0.02
Weibull	a = -0.003 ± 7.46E-4 b = -0.91 ± 0.001 k = 0.14 ± 5.19E-4 n = 0.98 ± 0.01	0.99	8.96E-6	0.006	7.85E-4
Hasibuan and Daud	a = 0.20 ± 3.13E-4 k = 0.08 ± 1.10E-4 n = 0.80 ± 9.43E-4	0.99	1.83E-5	0.004	0.02
Simplified ficks diffusion	a = 0.93 ± 3.37E-4 k = 0.15 ± 1.73E-4 c = 0.02 ± 3.30E-4	0.99	9.18E-6	0.003	0.01
720 W	Newton	k = 0.27 ± 0.01	0.97	0.002	0.05
	Page	k = 0.17 ± 0.02 n = 1.33 ± 0.06	0.99	5.76E-4	0.02
	Modified Page	k = 0.26 ± 0.06 n = 1.33 ± 0.06	0.99	5.76E-4	0.02
	Modified Page III	k = 1.08 ± 0.04 d = 1.72 ± 8.24 n = 0.86 ± 8.30	0.98	0.002	0.05
Henderson and Pabis	a = 1.00 ± 0.00 k = 0.27 ± 0.00	0.98	0.002	0.05	0.02
Two term exponential	a = 1.94 ± 0.05 k = 0.41 ± 0.01	0.99	4.50E-4	0.02	0.004
Wang and Singh	a = -0.20 ± 0.05 b = 0.01 ± 6.41E-4	0.98	0.002	0.04	0.02
Singh et al.	a = 0.03 ± 0.01 k = 0.24 ± 0.02	0.98	0.001	0.04	0.02

(continued on next page)

Table 5 (continued)

Model	Parameter	R ²	χ^2	RMSE	SSE
Approximation of Diffusion	a = 1.00 ± 0.00 b = 1.00 ± 0.00 k = 0.27 ± 0.02	0.97	0.003	0.06	0.03
Verma et al.	a = 1.34 ± 0.11 k = 0.35 ± 0.02 g = 1.81 ± 0.91892	0.99	3.73E-4	0.02	0.003
Ademiluyi Modified	a = 1.02 ± 0.02 k = 0.27 ± 0.01 n = 1.30 ± 0.07	0.99	5.97E-4	0.02	0.01
Weibull	a = 0.01 ± 0.02 b = -1.01 ± 0.03 k = 0.18 ± 0.02 n = 1.31 ± 0.10	0.99	6.62E-4	0.03	0.01
Combined two term and page	a = 0.46 ± 0.07 b = 0.53 ± 0.06 k = 0.03 ± 0.01 h = 0.20 ± 0.04 n = 1.92 ± 0.22	0.99	3.23E-4	0.017	0.002
Hasibuan and Daud	a = 0.19 ± 0.02 k = 0.07 ± 0.01 n = 1.11 ± 0.07	0.99	0.001	0.03	0.01
Simplified ficks diffusion	a = 1.13 ± 0.03 k = 0.24 ± 0.02 c = -0.08 ± 0.04	0.98	0.001	0.04	0.01

energy is 0.08 USD (Rs. 7 as per Govt. of Odisha, India tariff). Likewise, the cost of microwave drying from 180 W to 720 W ranges from 2.52 to 1.93 USD. Microwave drying consumes less energy due to uniform and faster heating with a higher drying rate and less time; hence, the cost of drying using a microwave will reduce the cost of the desired product (**Dehghannya et al., 2018**). The CO₂ emission ranges between 157.27 to 45.64 kg (CO₂) and 28.98 to 21.90 kg (CO₂) for evaporation of 1 kg of water of convective and microwave drying, respectively (Assuming 0.95 kg CO₂ is released on utilization of 1 kWh of electricity). The study was conducted by **Behera & Balasubramanian. (2021)**, which reported lower greenhouse gas emissions for hot air ovens and relatively little higher for microwave drying. The difference in drying time and parameters in both conditions might have resulted in such variation.

Open sun drying and air drying imparts no cost as the drying utilizes the energy of sun and wind for the evaporation process. The energy is free of cost, renewable, and is present in abundance compared to non-renewable sources, which utilize fossil fuel for the generation of electricity. Open sun drying takes less time compared to air drying as the drying rates were higher due to the utilization of the thermal energy of the sun during the process (**Agbede et al., 2020**). The studies were conducted in the colder months of the year when the temperature was low. Drying time will be shortened in the warmer months of the year when sun radiation will be more intense. Hence, the cost of drying will be reduced without any greenhouse gas (GHG) emission with the use of solar energy, adding sustainability to the process than hot air oven and microwave.

3.4. Influence of drying techniques on the functional group and crystal structure

The X-ray diffraction graphs for the open sun and air-drying conditions are represented in Fig. 5a. The graphs were compared with the standard JCPDS cards of newberyite (#19-0762), dittmarite (#20-0663), struvite (#71-2089), and magnesium pyrophosphate (#75-1055) to analyze the changes in the precipitates when subjected to different drying conditions (figs. S1–S3). The peaks of the graphs resembled struvite peaks, confirming the presence of struvite crystals. Moreover, the absence of any additional peaks confirms the purity of struvite. The FTIR plots (Fig. 6a) show the presence of P–O, N–H, O–H, Mg–O, N–H & O–H stretching, further confirming the XRD results of open sun and air drying (**Zaffar et al., 2023**). The crystal structure of the precipitate resembles struvite from the temperature ranging from 20 to 60 °C, but it changes when the temperature is increased to 80 °C (Fig. 5b). The air at 20 °C and 40 °C doesn't cause any change in the

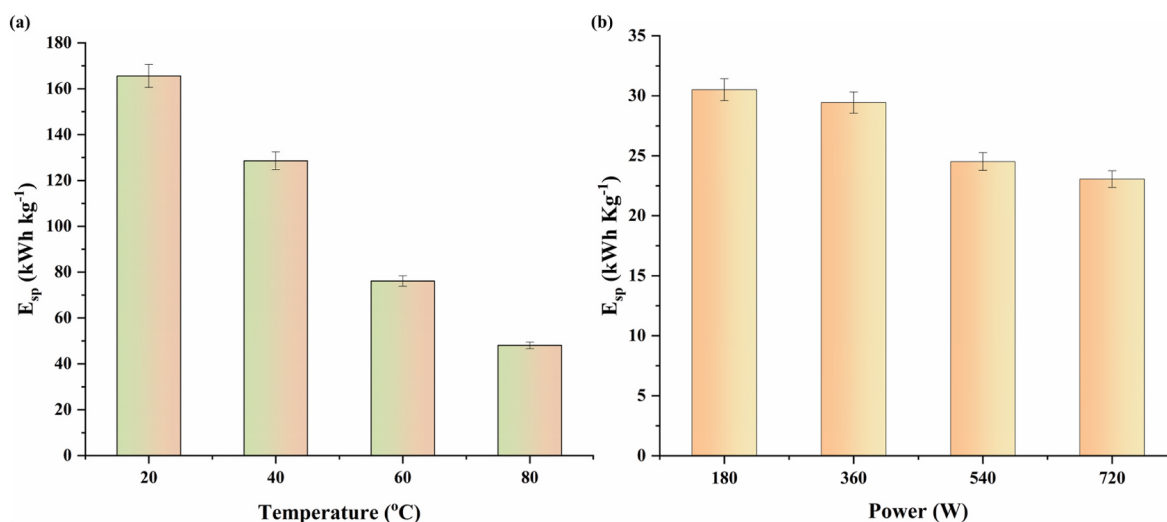


Fig. 4. Specific energy consumption during the drying of precipitate using different (a) Hot air oven temperature (b) Microwave power.

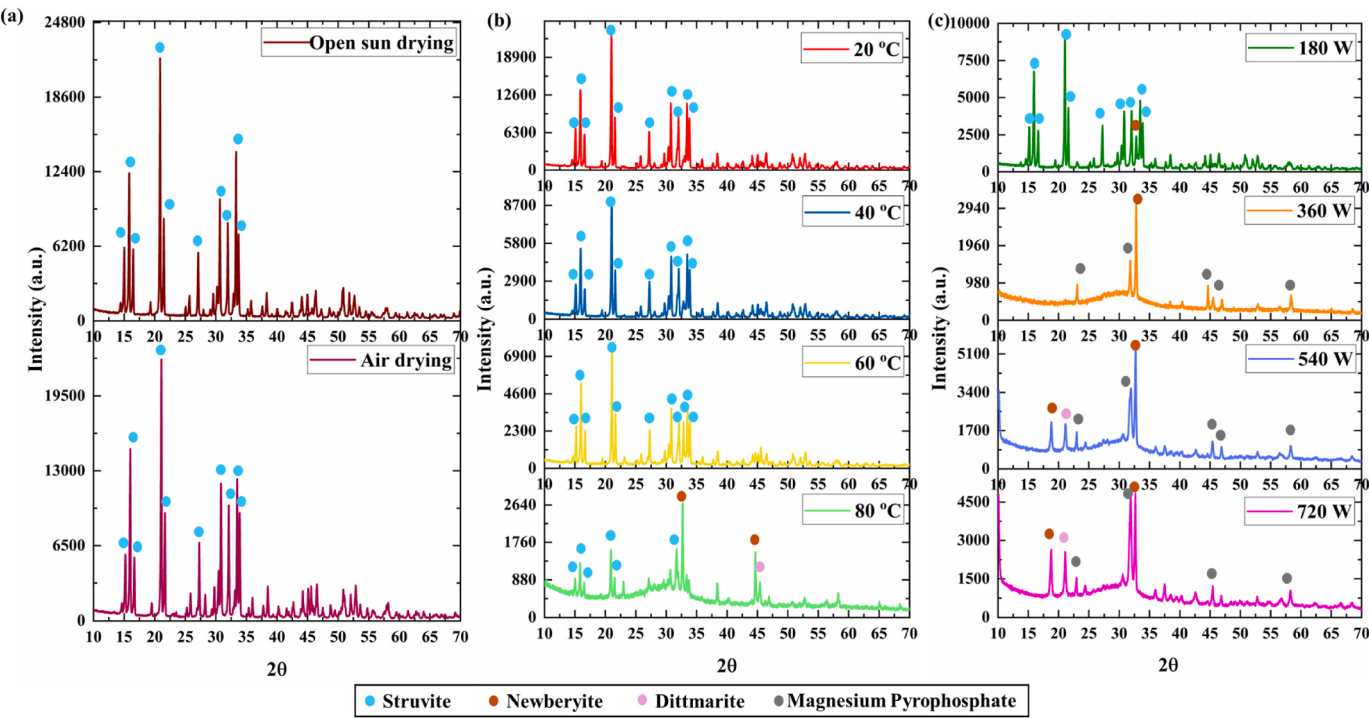


Fig. 5. X-ray diffraction graphs of precipitate dried in (a) Open sun drying and Air drying, (b) Conventional drying (20–80 °C), (c) Microwave drying (180–720 W) conditions.

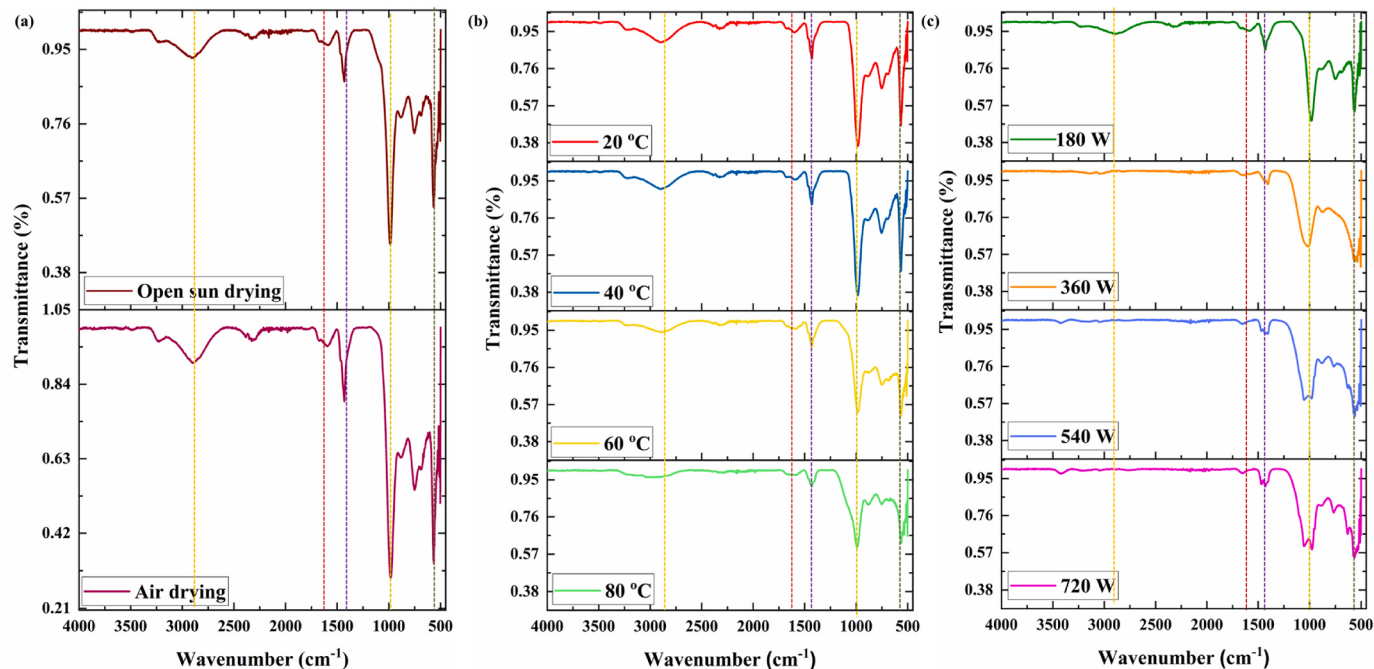


Fig. 6. FTIR spectra of precipitate dried in (a) Open sun drying and air drying, (b) Conventional drying (20–80 °C), (c) Microwave drying (180–720 W) conditions.

crystal structure of struvite as the temperature is not hot enough to remove water molecule. Novotny (2011) concluded no loss of mass or release of ammonia between 40 °C and 60 °C in isothermal conditions. On the contrary, Frost et al. (2004) reported that the decomposition of struvite can occur with the loss of ammonia even at less than 40 °C, followed by loss of water as the increases at a heating rate of 1° min⁻¹. Struvite becomes unstable above 50 °C, and depending on the time and temperature, it loses the water and ammonia molecules. Prolonged drying of struvite at 50 °C changes the molar ratio of Mg, N, and P in

struvite due to loss of nitrogen. This effect is immediately attained when heating occurs at higher temperatures. (Bayuseno and Schmahl, 2020). The FTIR graph of convective drying (Fig. 6b) concludes the decrease of intensity of O-H stretching at 60 °C followed by a decrease of both N-H and O-H bond at 80 °C. The increase in temperature to 60 °C and 80 °C results in the loss of 1 mol and 4 mol of water, respectively, along with ammonia molecules (Tansel et al., 2018). Farhana (2015) reported the loss of around 70% of ammonia at 60 °C, and the remaining ammonia is trapped in the 2D layered structure of magnesium and

phosphate. The conversion is intensified at higher temperatures and rapid heating, where the first decomposition of struvite to dittmarite can occur at 80 °C. The disintegration of the struvite crystals can be divided into three phases where the loss of occurs between 50 and 60 °C resulting in the formation of dittmarite, followed by the loss of ammonia after 60 °C forming newberryite and finally, loss of constituent water from the magnesium pyrophosphate above 250 °C (Saerens, 2020). Similarly, the introduction of steam at 80 °C completely transforms the struvite of 1 mm thickness to newberryite due to the rapid replacement of NH₃ molecules with H₂O (Farhana, 2015). Apart from temperature, higher drying duration can also lead to the conversion of struvite to amorphous phase at low temperatures (Tansel et al., 2018). Hence, both drying temperature and time determine the quality of the final struvite.

The change in the crystal structure of struvite with the increase of microwave power above 180 W (Fig. 5c) in microwave decomposes struvite by thermal and non-thermal methods. When the power is increased, the temperature of the air surrounding the precipitate increases, improving the removal of ammonia from the struvite crystals. Microwave offers non-surface drying, resulting in the propagation of heat throughout the material (Behera and Balasubramanian, 2021). High power generates more heat energy, which in turn produces local hot spots to release ammonia gas due to the pendulum vibration of ammonia and water molecules. The interaction between the microwave and dipole molecule (water) produces more heat along with higher microwave absorption at higher microwave power (Zhang et al., 2023). The change of struvite crystals was observed to occur more at 360 W than at 540 W and 720 W, as water plays an important role in the decomposition of struvite crystals. Due to the rapid evaporation of water, the ammonia release ratio becomes less. The FTIR graph further confirms the above results (Fig. 6c).

4. Conclusion

High production costs have hindered the scale-up of struvite technologies beyond the laboratory. Various methods are used to decrease the cost during precipitation, while limited knowledge is available to make the downstream processing cost-effective. The study reports the exploration of different drying techniques and a brief understanding of the influencing parameters that can make the process efficient and sustainable. The drying process exhibited a decreasing drying rate in all the cases, with effective diffusivity ranging from 10⁻⁹ to 10⁻⁷ m² s⁻¹. The drying time significantly decreased from 1440 to 90 min in a hot air oven and from 52 to 12 min in the microwave oven, attributed to increased power and temperature. The activation energy for conventional and microwave drying was 43.97 kJ mol⁻¹ and 54.14 W kg⁻¹, respectively. Further, the specific energy consumption, drying costs, and carbon dioxide emissions decreased with higher temperature and power, ranging from 165.55 to 48.05 kWh kg⁻¹ water for convective drying and from 30.50 to 23.06 kWh kg⁻¹ water for microwave drying. Kinetic modelling indicated that semi-theoretical and empirical models effectively described the drying mechanism under all conditions. Regardless of higher energy and cost efficiency, the use of microwave power above 180 W converts struvite into magnesium pyrophosphate, making it unsuitable for fertilizer applications. Therefore, solar drying is recommended as a suitable method with a drying time of 360 min, which can be further reduced with increased solar radiation and temperature. It is renewable, cost-free, readily available, and maintains the quality of struvite.

Funding Information

This research work was sponsored by the Department of Science and Technology (DST), Government of India (GOI) under the Agro-Technology Development Programme [File No. DST/TDT/Agro43/2020(G)] and DST NIDHI EIR scheme [File No. KIIT-TBI/INIDHI-EIR/10/07].

Ethical clearance

Not Applicable.

Consent to participate

Not Applicable.

Use of AI

During the preparation of this work, the authors have not used any AI-assisted technology.

Consent to publish

All authors allow the publication of the paper.

CRediT authorship contribution statement

Alisha Zaffar: Writing – original draft, Methodology, Formal analysis, Data curation, Conceptualization. **Sivaraman Jayaraman:** Writing – review & editing, Supervision. **Parag Prakash Sutar:** Writing – review & editing, Validation, Supervision. **Paramasivan Balasubramanian:** Writing – review & editing, Supervision, Resources, Project administration, Conceptualization.

Declaration of competing interest

All authors declare that there is no competing interest financially or personally, directly, or indirectly from the work reported in the study.

Data availability

Data will be made available on request.

Acknowledgment

The authors thank the Department of Biotechnology and Medical Engineering for providing the necessary research facility. The authors would like to acknowledge the fellowship support from Department of Science and Technology (DST), Government of India for the first author.

Appendix A. Supplementary data

Supplementary data to this article can be found online at <https://doi.org/10.1016/j.jenvman.2024.120665>.

References

- Ademiluyi, T., Oboho, E.O., Owudogu, M., 2008. Investigation into the thin layer drying models of Nigerian popcorn varieties. *Leonardo Electron. J. Pract. Technol.* 7 (13), 47–62.
- Agbede, O.O., Oke, E.O., Akinfenwa, S.I., Wahab, K.T., Ogundipe, S., Aworanti, O.A., Arinkoola, A.O., Agarry, S.E., Ogunleye, O.O., Osuolale, F.N., Babatunde, K.A., 2020. Thin layer drying of green microalgae (*Chlorella* sp.) paste biomass: drying characteristics, energy requirement and mathematical modeling. *Bioresoure Technology Reports* 11, 100467. <https://doi.org/10.1016/j.briteb.2020.100467>.
- Ameri, B., Hanini, S., Boumahdi, M., 2020. Influence of drying methods on the thermodynamic parameters, effective moisture diffusion and drying rate of wastewater sewage sludge. *Renew. Energy* 147, 1107–1119. <https://doi.org/10.1016/J.RENENE.2019.09.072>.
- Bagastyo, A.Y., Anggrainy, A.D., Khoiruddin, K., Ursada, R., Warmadewanthi, I.D.A.A., Wenten, I.G., 2022. Electrochemically-driven struvite recovery: Prospect and challenges for the application of magnesium sacrificial anode. *Separation and Purification Technology* 288, 120653. <https://doi.org/10.1016/J.SEPPUR.2022.120653>.
- Bayuseno, A.P., Schmahl, W.W., 2020. Thermal decomposition of struvite in water: qualitative and quantitative mineralogy analysis. *Environ. Technol.* 41, 3591–3597. <https://doi.org/10.1080/09593330.2019.1615558>.

- Behera, B., Balasubramanian, P., 2021. Experimental and modelling studies of convective and microwave drying kinetics for microalgae. *Bioresour. Technol.* 340, 125721. <https://doi.org/10.1016/J.BIOTECH.2021.125721>.
- Bennamoun, L., Chen, Z., Salema, A.A., Afzal, M.T., Canada, Q., 2014. Moisture diffusivity during microwave drying of wastewater sewage sludge. In: 2014 Montreal, Quebec Canada July 13–July 16, vol. 2014. American Society of Agricultural and Biological Engineers, p. 1.
- Bischel, H.N., Schindelholz, S., Schogler, M., Decrey, L., Buckley, C.A., Uderit, K.M., Kohn, T., 2016. Bacteria inactivation during the drying of struvite fertilizers produced from stored urine. *Environmental Science & Technology* 50, 13013–13023. <https://doi.org/10.1021/acs.est.6b03555>.
- Celma, A.R., Rojas, S., López, F., Montero, I., Miranda, T., 2007. Thin-layer drying behaviour of sludge of olive oil extraction. *J. Food Eng.* 80, 1261–1271. <https://doi.org/10.1016/J.JFOODENG.2006.09.020>.
- Chen, S., Yang, Y., Zheng, M., Cheng, X., Xu, K., Dou, X., 2020. Thermal decomposition of struvite pellet by microwave radiation and recycling of its product to remove ammonium and phosphate from urine. *Environ. Res.* 188, 109774. <https://doi.org/10.1016/j.enres.2020.109774>.
- Corzo, O., Bracho, N., Pereira, A., Vásquez, A., 2008. Weibull distribution for modeling air drying of coroba slices. *LWT - Food Sci. Technol. (Lebensmittel-Wissenschaft -Technol.)* 41, 2023–2028. <https://doi.org/10.1016/J.LWTF.2008.01.002>.
- Crank, J., 1975. Diffusion in a plane sheet. The mathematics of diffusion 47–48.
- Decrey, L., Uderit, K.M., Tilley, E., Peeson, B.M., Kohn, T., 2011. Fate of the pathogen indicators phage ΦX174 and Ascaris suum eggs during the production of struvite fertilizer from source-separated urine. *Water Res.* 45, 4960–4972. <https://doi.org/10.1016/j.watres.2011.06.042>.
- Dehghannya, J., Hosseiniar, S.H., Heshmati, M.K., 2018. Multi-stage continuous and intermittent microwave drying of quince fruit coupled with osmotic dehydration and low temperature hot air drying. *Innovative Food Sci. Emerging Technol.* 45, 132–151. <https://doi.org/10.1016/j.ifset.2017.10.007>.
- Dhurve, P., Kumar Arora, V., Kumar Yadav, D., Malakar, S., 2022. Drying kinetics, mass transfer parameters, and specific energy consumption analysis of watermelon seeds dried using the convective dryer. *Mater. Today Proc.* 59, 926–932. <https://doi.org/10.1016/j.matpr.2022.02.008>.
- Di Scala, K., Crapiste, G., 2008. Drying kinetics and quality changes during drying of red pepper. *LWT - Food Sci. Technol. (Lebensmittel-Wissenschaft -Technol.)* 41, 789–795. <https://doi.org/10.1016/J.LWTF.2007.06.007>.
- Doymaz, I., Smail, O., 2011. Drying characteristics of sweet cherry. *Food Bioprod. Process.* 89, 31–38. <https://doi.org/10.1016/J.FBP.2010.03.006>.
- Ertekin, C., Heybeli, N., 2014. Thin-layer infrared drying of mint leaves. *J. Food Process. Preserv.* 38, 1480–1490. <https://doi.org/10.1111/jfpp.12107>.
- Fang, H., Gao, L., Zhou, X., Yan, H., Wang, Y., Ji, H., 2023. Enhanced compressive strength of preheated limonite pellets with biomass-derived binders. *Adv. Powder Technol.* 34 (10), 104154. <https://doi.org/10.1016/j.apt.2023.104154>.
- Farhana, S., 2015. Thermal Decomposition of Struvite: A Novel Approach to Recover Ammonia from Wastewater Using Struvite Decomposition Products. Doctoral dissertation, University of British Columbia.
- Frost, R.L., Weier, M.L., Erickson, K.L., 2004. Thermal decomposition of struvite. *J. Therm. Anal. Calorim.* 76, 1025–1033.
- Ganesa Pillai, M., Goyal, S., Zawar, A., Kumar, M.S.A., Bakshi, H.S., Vijayalakshmi, C., Nakamura, K., 2022. An experimental study probing moisture kinetics and indices of microwave dried fecal sludge with an insight on real world applications. *Separ. Sci. Technol.* 57, 2227–2241. <https://doi.org/10.1080/01496395.2022.2041034>.
- Guo, J., Zheng, L., Li, Z., 2021. Microwave drying behavior, energy consumption, and mathematical modeling of sewage sludge in a novel pilot-scale microwave drying system. *Sci. Total Environ.* 777. <https://doi.org/10.1016/j.scitotenv.2021.146109>.
- Hii, C.L., Law, C.L., Cloke, M., 2008. Modelling of thin layer drying kinetics of cocoa beans during artificial and natural drying. *J. Eng. Sci. Technol.* 3 (1), 1–10.
- Horuz, E., Jaafar, H.J., Maskan, M., 2017. Ultrasonication as pretreatment for drying of tomato slices in a hot air-microwave hybrid oven. *Dry. Technol.* 35, 849–859. <https://doi.org/10.1080/07373937.2016.1222538>.
- Huang, Y.W., Chen, M.Q., 2017. Thin-layer isothermal drying kinetics of municipal sewage sludge based on two falling rate stages during hot-air-forced convection. *J. Therm. Anal. Calorim.* 129, 567–575. <https://doi.org/10.1007/s10973-017-6150-6>.
- Huang, H., Zhang, P., Xiao, J., Xiao, D., Gao, F., 2017. Repeatedly using the decomposition product of struvite by ultrasound stripping to remove ammonia nitrogen from landfill leachate. *Ultrason. Sonochem.* 38, 622–628. <https://doi.org/10.1016/J.ULTSONCH.2016.08.019>.
- Huang, W., Qiu, H., Zhang, Y., Zhang, F., Gao, L., Omran, M., Chen, G., 2023. Microstructure and phase transformation behavior of Al2O3-ZrO2 under microwave sintering. *Ceram. Int.* 49, 4855–4862. <https://doi.org/10.1016/j.ceramint.2022.09.376>.
- Inyang, U., Oboh, I., Etuk, B., 2017. Drying and the different techniques. *Int. J. Food Nutr. Sci.* 8 (1), 45–72.
- Inyang, U.E., Oboh, I.O., Etuk, B.R., 2018. Kinetic models for drying techniques—Food materials. *Adv. Chem. Eng. Sci.* 8, 27–48. <https://doi.org/10.4236/aces.2018.82003>.
- Kheto, A., Dhua, S., Nema, P.K., Sharanagat, V.S., 2021. Influence of drying temperature on quality attributes of bell pepper (*Capsicum annuum* L.): drying kinetics and modeling, rehydration, color, and antioxidant analysis. *J. Food Process. Eng.* 44 (11), 13880. <https://doi.org/10.1111/jfpe.13880>.
- Kim, A.H., Yu, A.C., El Abbadi, S.H., Lu, K., Chan, D., Appel, E.A., Cridle, C.S., 2021. More than a fertilizer: wastewater-derived struvite as a high value, sustainable fire retardant. *Green Chem.* 23, 4510–4523. <https://doi.org/10.1039/d1gc00826a>.
- Masmoudi, A., Ben Sik Ali, A., Dhaouadi, H., Mhiri, H., 2021. Draining solar drying of sewage sludge: experimental study and modeling. *Environ. Prog. Sustain. Energy* 40 (1), 13499. <https://doi.org/10.1002/ep.13499>.
- Mayer, B.K., Baker, L.A., Boyer, T.H., Drechsel, P., Gifford, M., Hanjra, M.A., Parameswaran, P., Stoltzfus, J., Westerhoff, P., Rittmann, B.E., 2016. Total value of phosphorus recovery. *Environ. Sci. Technol.* 50, 6606–6620. <https://doi.org/10.1021/acs.est.6b01239>.
- Midilli, A., Kucuk, H., Yapar, Z., 2002. A new model for single-layer drying. *Dry. Technol.* 20, 1503–1513. <https://doi.org/10.1081/DRT-120005864>.
- Noori, A.W., Royen, M.J., Hayday, J., 2021. Thin-layer mathematical modeling of apple slices drying, under open sun and cabinet solar dryer. *International Journal of Innovative Research and Scientific Studies* 4, 43–52. <https://doi.org/10.53894/ijirss.v4i2.55>.
- Novotny, C., 2011. Ammonia Removal and Recovery Using Heated Struvite as an Adsorbent. Doctoral dissertation, University of British Columbia.
- Olanipekun, B.F., Tunde-Akintunde, T.Y., Oyelade, O.J., Adebisi, M.G., Adenaya, T.A., 2015. Mathematical modeling of thin-layer pineapple drying. *J. Food Process. Preserv.* 39, 1431–1441. <https://doi.org/10.1111/jfpp.12362>.
- Omolola, A.O., Jideani, A.I.O., Kapila, P.F., 2014. Modeling microwave drying kinetics and moisture diffusivity of mabonde banana variety. *Int. J. Agric. Biol. Eng.* 7, 107–113. <https://doi.org/10.3965/j.ijabe.20140706.013>.
- Page, G.E., 1949. Factors Influencing the Maximum Rates of Air Drying Shelled Corn in Thin Layers. Purdue University.
- Pcock, J., Septien, S., Makununika, B.S.N., Velkushanova, K.V., Buckley, C.A., 2022. Convective drying kinetics of faecal sludge from VIP latrines. *Hel. Iyon* 8 (4). <https://doi.org/10.1016/j.heliyon.2022.e09221>.
- Praveen Kumar, D.G., Hebbar, H.U., Ramesh, M.N., 2006. Suitability of thin layer models for infrared-hot air-drying of onion slices. *LWT - Food Sci. Technol. (Lebensmittel-Wissenschaft -Technol.)* 39, 700–705. <https://doi.org/10.1016/J.LWTF.2005.03.021>.
- Preisner, M., Smol, M., Horttanainen, M., Deviatiin, I., Havukainen, J., Klavins, M., Ozola-Davidane, R., Kruopienė, J., Szatkowska, B., Appels, L., Houtmeyers, S., Roosalu, K., 2022. Indicators for resource recovery monitoring within the circular economy model implementation in the wastewater sector. *J. Environ. Manag.* 304, 114261. <https://doi.org/10.1016/J.JENVMAN.2021.114261>.
- Rabha, D.K., Muthukumar, P., Somayaji, C., 2017. Experimental investigation of thin layer drying kinetics of ghost chilli pepper (*Capsicum Chinense* Jacq.) dried in a forced convection solar tunnel dryer. *Renew. Energy* 105, 583–589. <https://doi.org/10.1016/j.renene.2016.12.091>.
- Rahman, M.S., Perera, C.O., Thebaud, C., 1997. Desorption isotherm and heat pump drying kinetics of peas. *Food Res. Int.* 30, 485–491. [https://doi.org/10.1016/S0963-9969\(98\)00009-X](https://doi.org/10.1016/S0963-9969(98)00009-X).
- Ruff-Salís, M., Brunnhöfer, N., Petit-Boix, A., Gabarrell, X., Guisasola, A., Villalba, G., 2020. Can wastewater feed cities? Determining the feasibility and environmental burdens of struvite recovery and reuse for urban regions. *Sci. Total Environ.* 737, 139783. <https://doi.org/10.1016/j.scitotenv.2020.139783>.
- Saerens, B., 2020. Thermal decomposition of struvite. *Journal of Thermal Analysis and Calorimetry*.
- Shaddel, S., Ucar, S., Andreassen, J.P., Sterhus, S.W., 2019. Engineering of struvite crystals by regulating supersaturation – correlation with phosphorus recovery, crystal morphology and process efficiency. *J. Environ. Chem. Eng.* 7, 102918. <https://doi.org/10.1016/J.JECE.2019.102918>.
- Silva, W.P., e Silva, C.M.D.P.S., Farias, V.S.O., Gomes, J.P., 2012. Diffusion models to describe the drying process of peeled bananas: optimization and simulation. *Dry. Technol.* 30, 164–174. <https://doi.org/10.1080/07373937.2011.628554>.
- Somorin, T., Fidalgo, B., Hassan, S., Sowale, A., Kolios, A., Parker, A., Williams, L., Collins, M., McAdam, E.J., Tyrrel, S., 2020. Non-isothermal drying kinetics of human feces. *Dry. Technol.* 38, 1819–1827. <https://doi.org/10.1080/07373937.2019.1670205>.
- Talboys, P.J., Heppell, J., Roose, T., Healey, J.R., Jones, D.L., Withers, P.J.A., 2016. Struvite: a slow-release fertiliser for sustainable phosphorus management? *Plant Soil* 401, 109–123. <https://doi.org/10.1007/s11104-015-2747-3>.
- Tansel, B., Lunn, G., Monje, O., 2018. Struvite formation and decomposition characteristics for ammonia and phosphorus recovery: a review of magnesium-ammonia-phosphate interactions. *Chemosphere* 194, 504–514. <https://doi.org/10.1016/j.chemosphere.2017.12.004>.
- Tinmaz Köse, E., Çelen, S., Çelik, S., 2019. Conventional and microwave drying of hydrocarbon cutting sludge. *Environ. Prog. Sustain. Energy* 38 (4), 13104. <https://doi.org/10.1002/ep.13104>.
- Tunde-Akintunde, T.Y., Ogunkakin, G.O., 2011. Influence of drying conditions on the effective moisture diffusivity and energy requirements during the drying of pretreated and untreated pumpkin. *Energy Conservation and Management* 52, 1107–1113. <https://doi.org/10.1016/J.ENCONMAN.2010.09.005>.
- Vega-Gálvez, A., Miranda, M., Díaz, L.P., Lopez, L., Rodriguez, K., Scala, K. Di, 2010. Effective moisture diffusivity determination and mathematical modelling of the drying curves of the olive-waste cake. *Bioresour. Technol.* 101, 7265–7270. <https://doi.org/10.1016/J.BIOTECH.2010.04.040>.
- Verma, L.R., Bucklin, R.A., Endan, J.B., Wratten, F.T., Member, A., Asae, A., 1985. Effects of drying air parameters on rice drying models. *Transactions of the ASAE* 28 (1), 296–301.
- Wang, P., Mohammed, D., Zhou, P., Lou, Z., Qian, P., Zhou, Q., 2019. Roof solar drying processes for sewage sludge within sandwich-like chamber bed. *Renewable Energy* 136, 1071–1081.
- Wang, Y., Tan, F., Gao, L., Zhou, X., Shi, Z., Li, N., 2023. Numerical simulation study on the effects of co-injection of pulverized coal and SPL (Spent Pot-Lining) into the blast furnace. *Fuel* 354, 129368. <https://doi.org/10.1016/j.fuel.2023.129368>.

- Westerman, P.W., White, G.M., Ross, I.J., Asae, A., 1973. Relative humidity effect on the high-temperature drying of shelled corn. *Transactions of the ASAE* 16 (6), 1136–1139.
- Wulyapash, W., Phongphiphat, A., Towprayoon, S., 2022. Comparative study of hot air drying and microwave drying for dewatered sludge. *Clean Technol. Environ. Policy* 24, 423–436. <https://doi.org/10.1007/s10098-021-02242-5>.
- Yaldız, O., Ertekin, C., Uzun, H.I., 2001. Mathematical modeling of thin layer solar drying of sultana grapes. *Energy* 26 (5), 457–465. [https://doi.org/10.1016/S0360-5442\(01\)00018-4](https://doi.org/10.1016/S0360-5442(01)00018-4).
- Yaldız, O., Ertekin, C., 2001. Thin layer solar drying of some vegetables. *Dry. Technol.* 19 (3–4), 583–597. <https://doi.org/10.1081/DRT-100103936>, 19, 583–597. *Drying Technology*.
- Yu, R., Geng, J., Ren, H., Wang, Y., Xu, K., 2013. Struvite pyrolysate recycling combined with dry pyrolysis for ammonium removal from wastewater. *Bioresour. Technol.* 132, 154–159. <https://doi.org/10.1016/J.BIOTECH.2013.01.015>.
- Zaffar, A., Krishnamoorthy, N., Nagaraj, N., Jayaraman, S., Paramasivan, B., 2023. Optimization and kinetic modeling of phosphate recovery as struvite by electrocoagulation from source-separated urine. *Environ. Sci. Pollut. Control Ser.* 30, 20721–20735. <https://doi.org/10.1007/s11356-022-23446-2>.
- Zhang, X.Y., Chen, M.Q., Huang, Y.W., Xue, F., 2016. Isothermal hot air drying behavior of municipal sewage sludge briquettes coupled with lignite additive. *Fuel* 171, 108–115. <https://doi.org/10.1016/j.fuel.2015.12.052>.
- Zhang, H.S., Chen, M.Q., Fu, B.A., Li, Q.H., 2021. Evaluation on microwave drying of waste paper towel with multi-magnetron and mode stirrer. *Dry. Technol.* 39, 882–895. <https://doi.org/10.1080/07373937.2020.1728306>.
- Zhang, J., Peng, Z., Luo, G., Tian, R., Rao, M., 2023. Microwave drying kinetics of chromium-rich electroplating sludge. *Metals* 13 (1), 87. <https://doi.org/10.3390/met13010087>.
- Zhou, J., Tian, C., Ren, C., Omran, M., Tang, J., Zhang, F., Chen, G., 2024. Dynamics characteristics and microstructure evolution of Sc₂O₃–ZrO₂ ceramic powders during microwave drying. *Ceram. Int.* <https://doi.org/10.1016/j.ceramint.2024.01.200>.